J Solid State Electrochem (2008) 12:1135–1141
DOI 10.1007/s10008-007-0460-8

ORIGINAL PAPER

Effect of nanoscale CeO_2 on PVDF-HFP-based nanocomposite porous polymer electrolytes for Li-ion batteries

G. Vijayakumar · S. N. Karthick · A. R. Sathiya Priya · S. Ramalingam · A. Subramania

Received: 21 May 2007 / Revised: 16 October 2007 / Accepted: 19 October 2007 / Published online: 16 November 2007

Abstract New poly (vinylidenefluoride-co-hexafluoro propylene) (PVDF-HFP)/CeO_2-based microcomposite porous polymer membranes (MCPPM) and nanocomposite porous polymer membranes (NCPPM) were prepared by phase inversion technique using *N*-methyl 2-pyrrolidone (NMP) as a solvent and deionized water as a nonsolvent. Phase inversion occurred on the MCPPM/NCPPM when it is treated by deionized water (nonsolvent). Microcomposite porous polymer electrolytes (MCPPE) and nanocomposite porous polymer electrolytes (NCPPE) were obtained from their composite porous polymer membranes when immersed in 1.0 M $LiClO_4$ in a mixture of ethylene carbonate/dimethyl carbonate (EC/DMC) (*v*/*v*=1:1) electrolyte solution. The structure and porous morphology of both composite porous polymer membranes was examined by scanning electron microscope (SEM) analysis. Thermal behavior of both MCPPM/NCPPM was investigated from DSC analysis. Optimized filler (8 wt% CeO_2) added to the NCPPM increases the porosity (72%) than MCPPM (59%). The results showed that the NCPPE has high electrolyte solution uptake (150%) and maximum ionic conductivity value of 2.47×10^{-3} S cm^{-1} at room temperature. The NCPPE (8 wt% CeO_2) between the lithium metal electrodes were found to have low interfacial resistance (760 Ω cm^2) and wide electrochemical stability up to 4.7 V (vs Li/Li^+) investigated by impedance spectra and linear sweep voltammetry (LSV), respectively. A prototype battery, which consists of NCPPE between the graphite anode and $LiCoO_2$ cathode, proves good cycling performance at a discharge rate of *C*/2 for Li-ion polymer batteries.

Keywords PVDF-HFP · SEM · CeO_2 · Ionic conductivity · Li-ion polymer batteries

G. Vijayakumar · S. N. Karthick · A. R. Sathiya Priya · S. Ramalingam · A. Subramania (✉)
Advanced Materials Research Laboratory,
Department of Industrial Chemistry, Alagappa University,
Karaikudi, 630 003, India
e-mail: ngvijayakumar@yahoo.co.in

Introduction

Solvent-free polymer electrolytes have been attracting attention as safer alternatives to liquid electrolytes for use in lithium secondary batteries and other electrochemical devices [1]. These polymer electrolytes act as an ionic conductor and also as an electrical insulator (separator) between the positive and negative electrodes. Hence, the control of the miscibility and stability between the liquid electrolytes and the host polymer itself has become one of the prominent factors for gel electrolytes [2]. Generally, GPE is composed of a host polymer material by injecting liquid electrolytes into the small pores of the polymer matrixes. Liquid electrolytes are prepared by blending organic solvents, such as ethylene carbonate (EC), propylene carbonate (PC), dimethyl carbonate (DMC), and diethyl carbonate (DEC) with salts [3]. These electrolytes can exhibit high ionic conductivity as high as 10^{-3} S cm^{-1} [2]. But with long-time usage, the organic liquid electrolyte solvents may leak from the polymer electrolyte, which causes a fall in ion conductivity with damage to the lithium electrode and other components. To resolve these problems, the effect of inorganic oxides such as SiO_2, MgO, CeO_2, and Al_2O_3 [4–7] on the electrochemical properties of plasticized polymer electrolytes has been studied. It has been shown that ceramic fillers may greatly influence the properties of polymer electrolyte. Recently, PVDF-HFP-based polymer electrolyte exhibits excellent mechanical and

chemical stability [8]. The microporous structure of the host polymer matrix is one convenient pathway for ionic transport and enhances conduction. PVDF-HFP copolymer-based polymer electrolyte is the most commonly commercialized plastic lithium ion batteries (PLiON™) by Telcordia Technologies (formerly Bellcore) since Gozdz et al. found the preparation process of porous membrane [9–13]. However, in the process, the DBP extraction step is inconvenient because it increases the cost of the preparation. Some researchers have reported an alternative method to form the porous structure by the phase inversion technique [8, 14–16]. Uvarov et al. has studied the effect of adding some rare earth oxide ceramics such as CeO_2, SiO_2, fly ash, and Eu_2O_3 as dispersoids, and verified the fact that other than γ-Al_2O_3, the abovementioned dispersoids also help in achieving the modest enhancement in the ionic conductivity of the composite solid electrolytes [17]. Nonetheless, micro/nanoscale CeO_2 filler incorporated on the PVDF-HFP polymer matrix, their morphology, and electrochemical behavior of the micro/nanocomposite porous polymer electrolyte has not yet been studied.

In the present study, we focus on a new PVDF-HFP/CeO_2 nanocomposite porous polymer electrolyte (NCPPE) and seek to determine the importance of its structural and electrochemical properties compared to the microcomposite porous polymer electrolytes (MCPPE). At the first step, micro/nanocomposite porous PVDF-HFP/CeO_2 membranes are obtained by adopting the phase inversion technique and also by changing the CeO_2 filler (wt%) content. NMP is used as a good solvent, and deionized water is used as a nonsolvent. At the second step, activation of the composite porous polymer membrane by immersing into the liquid electrolyte solution of 1.0 M $LiClO_4$ a mixture of EC/DMC (v/v=1:1) to obtain MCPPE/NCPPE. Morphology of the composite porous polymer membrane and electrochemical properties of the MCPPE/NCPPE are described herein. Moreover, the effect of nanoscale CeO_2 filler on the NCPPE is attracting more attention and determination of its optimal filler content shows the good structural and electrochemical properties for rechargeable lithium ion batteries.

Experimental

PVDF-HFP (Mw=400,000) as a host polymer matrix, microscale and/or nanoscale cerium oxide (CeO_2, 5 μm and 10 nm) inert ceramic filler and lithium perchlorate ($LiClO_4$) as an electrolyte salt was purchased from Aldrich (USA). The host polymer was dried at 80 °C under vacuum for 12 h. The $LiClO_4$ salt and ceramic filler were used after drying at 100 °C under vacuum for 24 h. NMP was obtained from E-Merck and used as received. EC and DMC obtained from Aldrich (USA) were used as plasticizer without further treatment.

A certain amount of PVDF-HFP was dissolved in the NMP solvent with constant stirring to form a homogeneous solution. Then the CeO_2 filler (micro/nanoscale filler) was added to the polymer solution and stirred continuously for 24 h. The resulting homogenous viscous slurry was cast on a newly cleaned glass plate and the desired thickness was made by doctor blade. The glass plate was put into large excess of deionized water for 2 h to extract the solvent and phase inversion occurred. The resulting MCPPM and NCPPM were dried under vacuum at 80 °C for 6 h. Finally, a dimensionally stable and solvent free of both composite porous polymer membranes were obtained with a thickness ranging from 100 to 150 μm.

The morphological properties of the dry composite porous polymer membranes were examined by means of a scanning electron microscopy JEOL-SEM (Model JSM-840A) instrument with accelerating voltage range of 20 kV. Thermal property of the PVdF-HFP/CeO_2 composite porous membranes was investigated using a Perkin Elmer (Model Pyris 6DSC) instrument; then, the samples were dried under vacuum at 80 °C for 24 h without lithium salt electrolyte content. The measurement was carried out with the heating rate of 10 °C/min at nitrogen atmosphere. Crystallinity (X_c [%]) of the composite porous polymer membrane is calculated as follows:

$$X_c[\%] = \frac{\Delta H_m}{\Delta H_m^{\Phi}} \times 100$$

where, ΔH_m^{Φ} is the crystalline melting heat of pure α-PVDF, 104.7 J g^{-1} [18], ΔH_m is the heat of melting for the PVDF-HFP membrane. The porosity of the composite membrane was measured by immersing the membrane into *n*-butanol for 1 h, weighing the membrane before and after absorption of *n*-butanol, and then calculated using the following equation:

$$\rho[\%] = \frac{W_a/\rho_a}{W_a/\rho_a + W_p\Big/\rho_p} \times 100$$

where W_p is the weight of dry membranes, W_a is the weight of *n*-butanol absorbed in the wet membrane, ρ_a is the density of *n*-butanol, and ρ_p is the density of membrane. The porous membrane liquid electrolyte solution uptake was measured as a function of the soaking time in 1.0 M $LiClO_4$–EC/DMC (v/v=1:1) to activate the porous polymer membrane for 6 h and calculated as follows:

$$\text{Solution uptake weight}\,[\text{wt }\%] = \frac{W_t - W_o}{W_o} \times 100$$

where W_t and W_o are the weight of the wet and dry polymer membranes, respectively.

A liquid electrolyte solution of 1.0 M $LiClO_4$ dissolved in the mixture of EC/DMC (v/v=1:1) was used as the liquid

electrolyte. The composite membrane was prepared through two steps. First, the composite porous membrane was wetted completely by dipping it into the liquid electrolyte for 6 h. Then, the wetted membrane was pressed lightly between two sheets of filter papers to remove excess liquid electrolyte on the surface. To measure ionic conductivity, the composite electrolyte was sandwiched between two stainless steel nonblocking electrodes. Ionic conductivity of the various composite porous polymer electrolytes were measured by LCR HiTESTER (HIOKI 3522-50) using a wide frequency range of 10 Hz–100 KHz at an applied potential of 10 mV. Temperature dependence of conductivity was studied at the temperature range of 25 to 80 °C. The ionic conductivity of the various polymer electrolytes were determined using conductivity equation:

$$\sigma = \frac{t}{A \times R_b}$$

where σ the conductivity, t is the thickness of the polymer electrolyte film, R_b and A are the bulk resistance and cross-sectional area of the composite porous electrolyte membrane, respectively. All the experiments were carried out under inert argon gas-filled glove box to prevent the composite porous polymer electrolyte from moisture. The interfacial stability between lithium and polymer electrolyte was confirmed from the AC-impedance spectrum of the Li/polymer electrolyte/Li a nonblocking electrode in the range of 10 Hz–1 MHz, using the EG & G electrochemical analyzer at the amplitude of 10 mV for different storage times. The electrochemical stability window of the polymer electrolyte was determined by running a linear sweep voltammetry. It was performed on SS working electrode with lithium as both counter and reference electrode using the same EG & G electrochemical analyzer and was operated in the potential range of 2.0 to 5.5 V vs Li/Li^+ at a scan rate of 1.0 mV s^{-1}.

A coin type lithium ion cell was assembled by sandwiching the composite polymer electrolyte between a graphite anode and a $LiCoO_2$ cathode. The cell was assembled and then sealed under vacuum in a glove box filled with argon. The cell performance of the composite polymer electrolyte was evaluated galvanostatically using WonATech battery cycle life tester. At the $C/2$ rate, the test was carried out at a constant current density of 0.25 mA cm^{-2} and cutoff voltage of 3.0 and 4.2 V. All the electrochemical measurements were performed under inert argon gas atmosphere.

Results and discussions

Morphology and thermal studies

The morphology of microcomposite/nanocomposite polymer membranes was examined by SEM and selected samples are shown in Fig. 1a–c. Figure 1a shows the surface SEM images revealing that optimized MCPPM (8 wt% CeO_2) exhibits a compact structure and irregular pores are seen, whereas in the case of optimized (8 wt% CeO_2) NCPPM, a sponge-like structure is seen (Fig. 1b). In the latter case, one or two places exhibit micropores (5 μm) and also some small pores (1 μm). It is interesting to note that we found that the diameter of the pores increases with

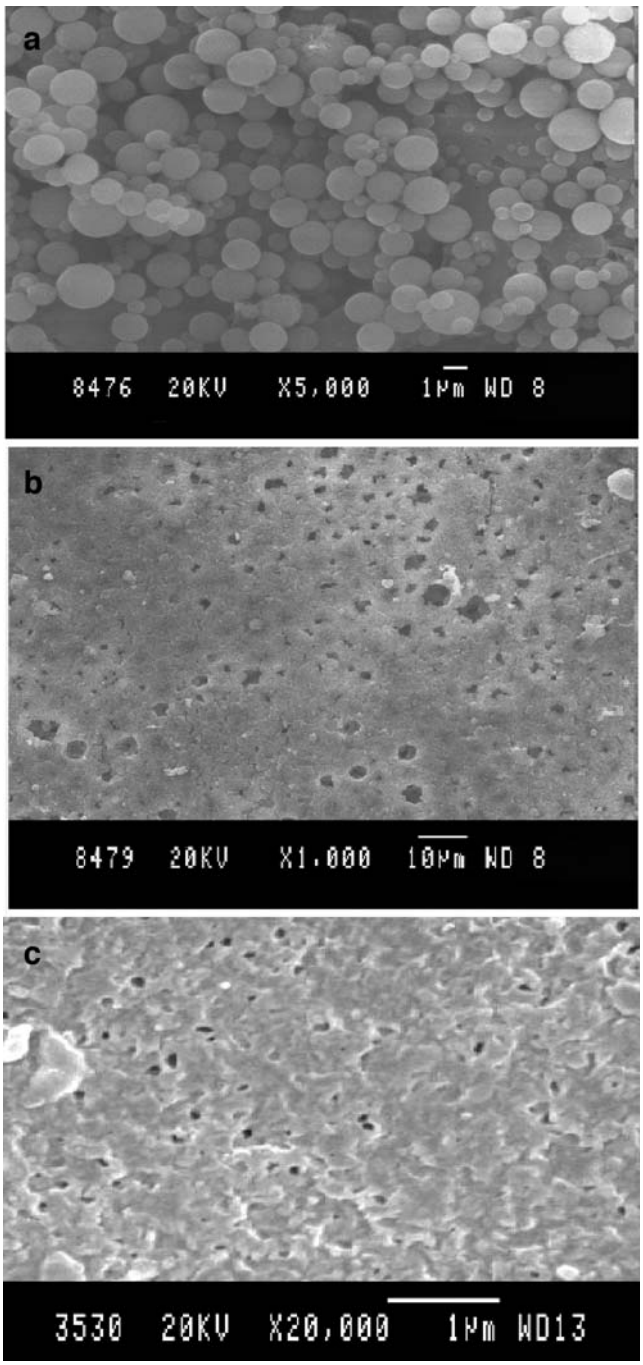

Fig. 1 SEM image surface view of PVDF-HFP/CeO_2 membrane of optimized filler added **a** MCPPM, **b** NCPPM, and **c** 10 wt% CeO_2 nanoscale filler-added NCPPM

the increase of the nanoscale filler (>8 wt%) content during the phase inversion process. Furthermore, the addition of filler (10 wt% CeO_2) concentration on the polymer matrix leads to a more roughened surface due to the growth of aggregates and shows irregular porous morphology (Fig. 1c). The porosity of microcomposite and nanocomposite porous polymer membranes is given in Tables 1 and 2. It is quite obviously observed that the addition of filler increased the porosity of the composite polymer membranes. However, porosity and liquid electrolyte solution uptake of the composite porous polymer membranes decreased when adding 10 wt% of CeO_2. Liquid electrolyte solution uptake of MCPPM shows a maximum of 92% and NCPPM reaches a maximum solution uptake of 150%, as clearly seen from the Table 2. It implies that the nanocomposite porous polymer membrane enhances the liquid electrolyte solution uptake due to the higher affinity of the filler toward the solvents of the (EC/DMC) liquid electrolyte solution.

Figure 2 illustrates the DSC thermogram of both composite porous polymer membranes with two different particle size filler (8 wt% CeO_2) contents. Nanoscale filler incorporation into the polymer matrix have lower melting temperature (T_m=142.2 °C) and heat of melting (ΔH_m= 25.17 J g^{-1}) than microscale filler incorporation into the polymer matrix (T_m=143.3 °C; ΔH_m=35.1 J g^{-1}). It is further evident from the Tables 1 and 2 that the addition of nanoscale filler causes a decreased trend of crystallinity below 10 wt% filler than the microscale filler content on the polymer matrix.

Electrochemical studies

Figure 3 shows a typical AC-impedance spectrum of the optimized filler incorporated with NCPPE and MCPPE at room temperature. The NCPPE (PVDF-HFP/8 wt% CeO_2–1.0 M $LiClO_4$ in a mixture of EC/DMC [*v*/*v*=1:1]) has higher ionic conductivity (2.47×10^{-3} S cm^{-1}) and one order magnitude increased than the ionic conductivity of MCPPE (3.90×10^{-4} S cm^{-1}). This indicates that the amount of nanoscale filler on the polymer matrix (NCPPM) during the phase inversion process enhance the porosity and uptake of electrolyte solution due to the surface to volume ratio. The above results are very essential factors for transporting of charge carriers in the polymer network to enhance the conductivity. On the other hand, the enhancement of ionic conductivity would be expected due to CeO_2, which interacts with either or both the anion and cation, thereby reducing ion pairing and increases the number of charge carriers [6]. Jacob et al. reported, using CeO_2 as dispersoids particle rather than γ-Al_2O_3, that the effect seems very similar to alumina-dispersed composites electrolytes. The pronounced changes in conductivity values have been observed at all temperatures [19]. Ionic conductivity of the NCPPE has a higher value than the Al_2O_3, MCM-41, and SBA-15 filler particles on the PVDF-HFP-based composite microporous polymer electrolytes

Table 1 Properties of MCPPM [melting temperature (T_m [°C]), heat of melting (ΔH_m [J g^{-1}]), crystallinity (X_c [%]), porosity (ρ [%]), solution uptake (wt%), and ionic conductivity (at 25 °C) of the MCPPE

Microscale CeO_2 filler (wt%)	MCPPM				MCPPE	
	T_m (°C)	ΔH_m (J g^{-1})	X_c (%)	ρ (%)	Solution uptake (wt%)	$\sigma\times10^{-3}$ (S cm^{-1})
2	144.0	41.2	39.35	44	64	0.23
4	143.8	40.9	39.06	46	76	0.29
6	143.5.	38.2	36.48	52	82	0.36
8	143.3	35.1	33.52	59	92	0.39
10	143.9	32.0	35.56	47	79	0.31

Table 2 Properties of NCPPM [melting temperature (T_m [°C]), heat of melting (ΔH_m [J g^{-1}]), crystallinity (X_c [%]), porosity (ρ [%]), solution uptake (wt%), and ionic conductivity (at 25 °C) of the NCPPE

Nanoscale CeO_2 filler (wt%)	NCPPM				NCPPE	
	T_m (°C)	ΔH_m (J g^{-1})	X_c (%)	ρ (%)	Solution uptake (wt%)	$\sigma\times10^{-3}$ (S cm^{-1})
2	143.2	30.81	29.41	58	124	1.56
4	143.1	28.72	27.43	63	132	1.62
6	142.7	27.33	26.10	66	146	1.86
8	142.2	25.17	24.04	72	150	2.47
10	143.1	26.54	25.34	64	132	1.71

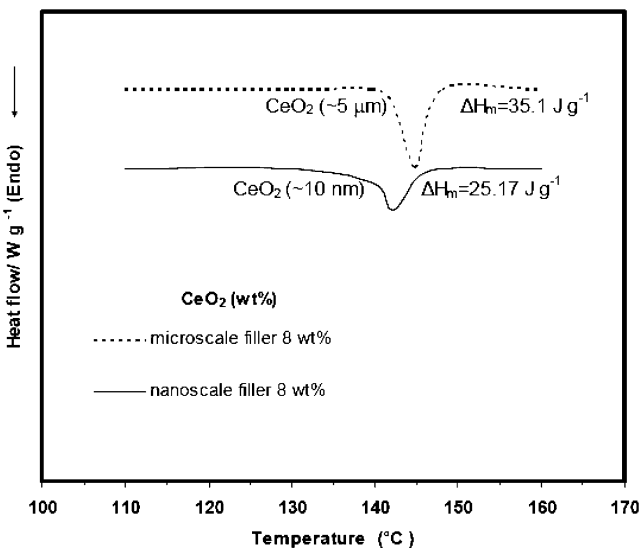

Fig. 2 DSC thermogram of PVDF-HFP/CeO_2 composite membrane MCPPM (**a**) and NCPPM (**b**)

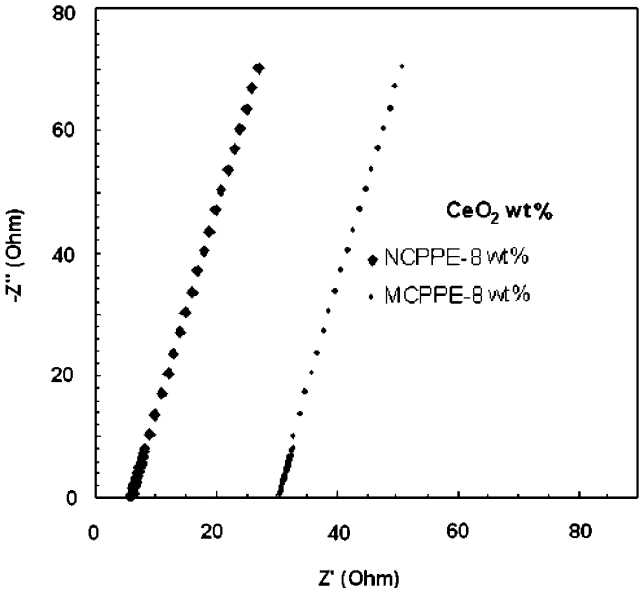

Fig. 3 AC-impedance spectra for the optimized filler-added MCPPE and NCPPE at room temperature

[20, 21]. As clearly seen from the Table 1, the ionic conductivity value is increased with the increase of filler content up to 8 wt% CeO_2 concentrations. It is high enough for practical application in Li-ion polymer batteries. In addition, 10 wt% CeO_2 filler on the polymer electrolyte (NCPPE) causes the rapid decrease in conductivity, which implies that an increase in the dilution effect predominates and the conductivity decreases continuously [22]. An Arrhenius plot of Log σ vs 1,000/T for the MCPPE and NCPPE were obtained by immersing the composite porous membrane in liquid electrolyte solution and are shown in Fig. 4. It is found that the 8 wt% CeO_2–NCPPE exhibits higher Log σ value among the systems studied over the whole temperature ranges of 298–353 K. Moreover, the conductivity value also increases with the increase of filler content up to 8 wt% and then decreases with increase of filler content. This is because the optimum concentration of CeO_2 is achieved only in the concentration region of 8 wt% of CeO_2. This effect could perhaps be quantitatively understood by the space charge effect [23], whereas the highly conducting behavior can be attributed to the carrier enhancement in the space charge layer close to the interface, and the nanoscale filler effect is very similar to the Al_2O_3 particles that are present in the polymer electrolyte matrix. Generally, it seems that the polymer electrolyte quite obviously observed in the temperature increases with the increase of ionic conductivity and also increases with the increase of filler content [24] up to some extent. The plot suggests that the ion transports in polymer electrolytes are associated with polymer segmental motion. The temperature depends on the ionic conductivity of the polymer electrolyte and obeys the Arrhenius behavior.

Figure 5 shows the time evolution of interfacial resistance of both composite porous polymer electrolytes and their impedance spectral values measured from the Li/polymer electrolyte (MCPPE or NCPPE)/Li symmetrical cell kept on open circuit for different storage times. NCPPE are obviously distinguished from those of MCPPE. The latter case exhibits higher interfacial resistance of 1,420 Ω cm^2 after 600 h even with the optimal filler content in the polymer matrix. It is due to the increase of the passivation layer through the continuous reaction with the electrode/electrolyte components as the time proceeds. Contrary to the MCPPE, the nanocomposite porous polymer electrolyte behaves more stably and has less interfacial resistance of 760 Ω cm^2 at the same storage time of 600 h. The higher interfacial resistance for the MCPPE based on the growth of the passivation layers seems to be associated with the growth of the passivation layer on the lithium electrode

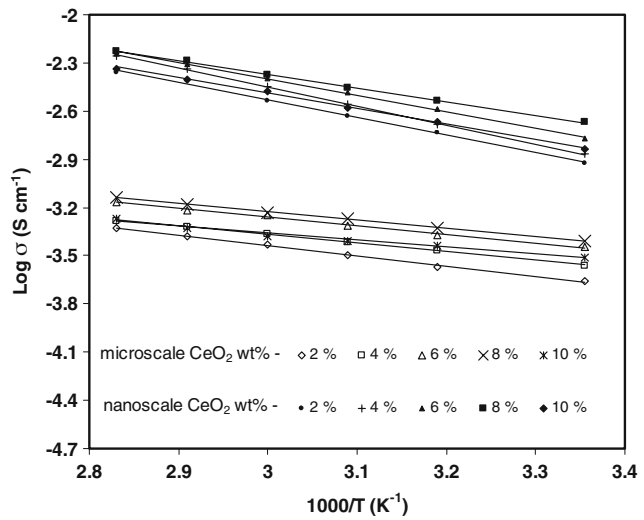

Fig. 4 Arrhenius plot of MCPPE and NCPPE filled with different wt% of CeO_2 filler

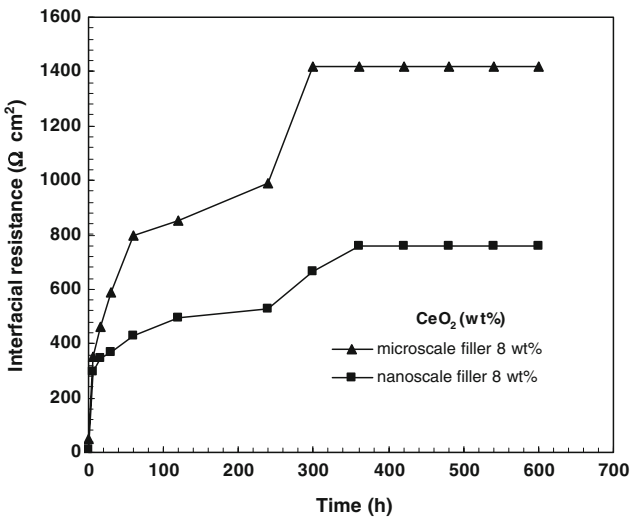

Fig. 5 Interfacial resistance of optimized filler-added MCPPE and NCPPE

surface and the degradation of the physical contact between the polymer electrolyte and lithium electrode [25, 26]. From this, it is concluded that the higher interfacial stability of NCPPE, when compared with that of an analogous, microcomposite porous polymer electrolyte clearly shows the superior behavior of the former over the latter. Figure 6 shows the schematic model of the Li/CPE (composite polymer electrolyte) interface [27].

Figure 7 displays the current–voltage response of the composite porous polymer electrolytes using SS as a working electrode and lithium metal as a reference electrode measured between the potential ranges of 2.0 to 5.5 V with a scan rate of 1.0 mV s^{-1}. The onset current flow is associated with the decomposition voltage of the composite porous polymer electrolyte. The decomposition of NCPPE is found to be low, no electrochemical oxidation occurs when the voltage is below 4.7 V (vs Li/Li^+) and the current sharply increases when the voltage is about 4.8 V. The decomposition voltage of MCPPE is about 4.5 V (vs Li/Li^+). Thus, the oxidation stability of the NCPPE is suitable for high-voltage cathode materials such as $LiNiO_2$, $LiCoO_2$, and $LiMn_2O_4$.

A prototype graphite/polymer electrolyte (NCPPE/MCPPE)/$LiCoO_2$ coin type cell was fabricated to evaluate the cycling performance. $LiCoO_2$ is the widely used cathode material for conventional lithium ion batteries. The cell was subjected to the cycle test with a cutoff voltage of 4.2 V for the upper limit and 3.0 V for the lower limit. Figure 8 displays the curve of the discharge capacity vs cycle number for 50 cycles. The cell delivered a discharge capacity of 123 mAh g^{-1} for the initial cycle at the *C*/2 rate. The Coulumbic efficiency is more than 90% after 10 cycles, and the discharge capacity after 30 cycles is about 86% of the initial discharge capacity for the NCPPE system. In contrast, MCPPE shows that the initial discharge capacity (124 mAh g^{-1}) of the cell is higher and declines faster (Coulumbic efficiency is 59% for 30 cycles) during the cycling test compared with NCPPE. The NCPPE showed relatively stable discharge properties, having little capacity fade under constant current and constant voltage conditions at the *C*/2 rate; it is suitable to give good performance for the Li-ion polymer batteries.

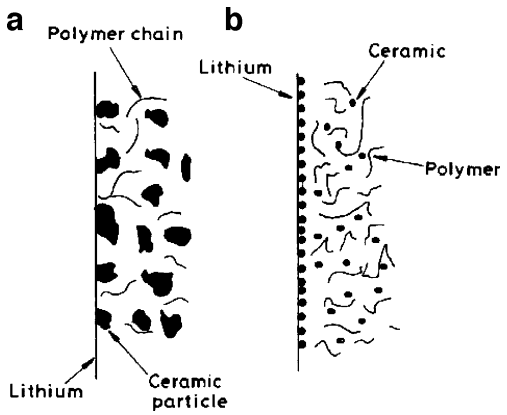

Fig. 6 The schematic representation of composite polymer electrolytes with the inert filler of different sizes (derived from Kumar and Scanlon [27]). **a** Micron-sized particle. **b** Nanosized particle

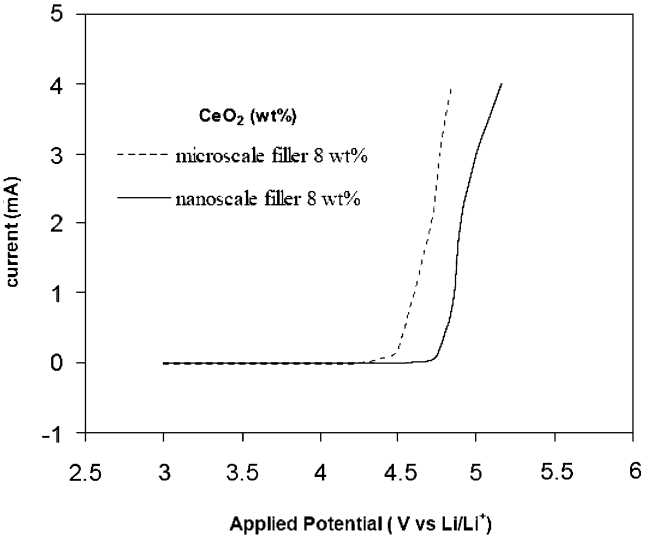

Fig. 7 Linear sweep voltammetry of MCPPE (**a**) and NCPPE (**b**)

Conclusions

Nanocomposite porous polymer electrolyte prepared successfully by immersing the nanocomposite porous polymer membrane in 1 M $LiClO_4$ in a mixture of EC-DMC (1:1 *v*/*v*) electrolyte solution. The ionic conductivity of the NCPPE based on 8 wt% CeO_2 reached a maximum of 2.47×10^{-3} S cm^{-1} at room temperature. An Arrhenius plot also implies that the ion transport is also due to the influence of the filler on the composite porous polymer electrolyte and also

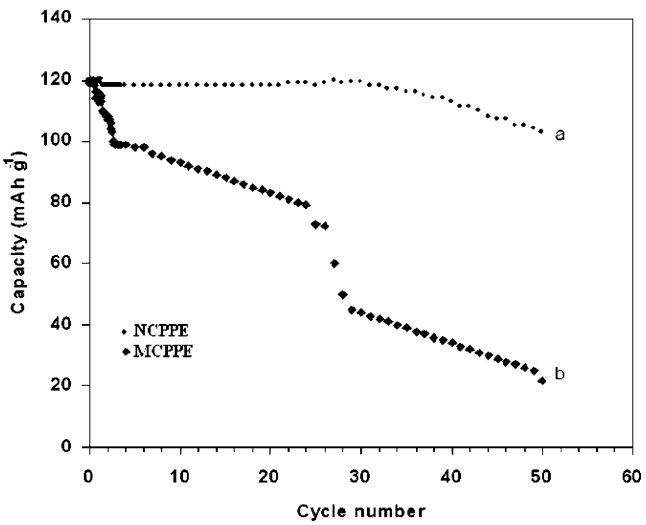

Fig. 8 Cycling performance of the optimized filler-added MCPPE and NCPPE with discharge rate of *C*/2

increases the segmental motion. The incorporation of filler nanoparticles not only reduces the interfacial resistance but also provides better electrochemical stability window of 4.7 V and good cycling performance during charge/discharge at the *C*/2 rate. From these results, optimized filler-added NCPPE is considered to give the best performance for application in lithium ion polymer batteries.

Acknowledgement The authors gratefully acknowledge the University Grants Commission (UGC), New Delhi for giving the financial support to carry out this work.

References

1. Gray FM (1997) Polymer electrolytes. RSC Monographs, The Royal Society of Chemistry, London
2. Song JY, Wang YY, Wan CC (1999) J Power Sources 77:183
3. Tarascon J, Gozdz A, Schmutz C, Shokoohi F, Warren P (1996) Solid State Ion 86:49
4. Lee KH, Lee YG, Park JK, Seung DY (2000) Solid State Ion 133:257
5. Prosini PP, Villano P, Carewska M (2002) Electrochim Acta 48:227
6. Rajendran S, Mahendran O, Kannan R (2002) J Phys Chem Solids 63:303
7. Appetecchi GB, Romagnoli P, Scrosati B (2001) Electrochem Commun 3:281
8. Magistris A, Mustarelli P, Parazzoli F, Quartarone E, Piaggio P, Bottino A (2001) J Power Sources 97:657
9. Xu W, Siow KS, Gao Z, Lee SY (1999) J Electrochem Soc 146:4410
10. Qiu X, Li W, Zhang S, Liang H, Zhu W (2003) J Electrochem Soc 150:A917
11. Huang H, Wunder SL (2001) J Power Sources 97:649
12. Gozdz AS, Schmutz CN, Tarascon JM (1994) US Patent 5296138
13. Gozdz AS, Schmutz CN, Tarascon JM, Warren PC (1996) US Patent 5540741
14. Zhang SS, Xu K, Foster DL, Ervin MH, Jow TR (2004) J Power Sources 125:114
15. Boudin F, Andriet X, Jehoulet C, Olsen M (1999) J Power Sources 81:804
16. Stephan AM, Saito Y (2002) Solid State Ion 148:475
17. Uvarov NF, Isupov VP, Sharma V, Shukla AK (1992) Solid State Ion 51:41
18. Rosenberg Y, Sigmann A, Narkis M, Shkolnik S (1991) J Appl Polym Sci 43:535
19. Jacob MME, Rajendran S, Gangadharan R, Siluvai Michael M, Sahaya Prabaharan SR (1996) Solid State Ion 86:595
20. Li Z, Su G, Wang X, Gao D (2005) Solid State Ion 176:1903
21. Jiang YX, Chen ZF, Zhuang QC, Xu JM, Dong QF, Huang L, Sun SG (2006) J Power Sources 46:1320
22. Qian X, Gu N, Cheng Z, Yang X, Wang E, Dong S (2001) Electrochim Acta 46:1829
23. Maier J (1994) Ber Bunsenges Physik Chem 88:1057
24. Liu Y, Lee JY, Hong L (2004) J Power Sources 129:303
25. Kim JR, Choi SW, Jo SM, Lee WS, Kim BC (2004) Electrochim Acta 50:69
26. Appetecchi GB, Croce F, Scrosati B (1995) Electrochim Acta 40:991
27. Kumar B, Scanlon LG (1994) J Power Sources 52:261